

# Morphotectonic Analysis of Sub-Basins along the North Termination of Anar Fault, Yazd Block, Iran

E. Gholami<sup>a,\*</sup>, P. Vaghari<sup>a</sup>, M. M. Khatib<sup>a</sup>, and A. Faghih<sup>b</sup>

<sup>a</sup> University of Birjand, Geology Department, Birjand, Southern Khorasan, 9717434765 Iran

<sup>b</sup> Shiraz University, College of Sciences, Department of Earth Sciences, Shiraz, Fars, 7194684334 Iran

\*e-mail: egholami@birjand.ac.ir

Received May 17, 2023; revised June 7, 2023; accepted June 16, 2023

**Abstract**—The morphotectonic analysis is a significant tool to assess the tectonic activity in the study area. The Anar fault system with strike-slip mechanism and length of ~200 km associated with numerous minor faults represents an important tectonic feature in the Yazd block. Despite the lack of data of large earthquakes ( $M \geq 4.5$ ) along the Anar fault system (AFS), there is much notable Quaternary geomorphic evidence which highlight its recent tectonic activity. In our study we used geomorphic indicators such as drainage basin Asymmetry Factor (Af), Stream Length-gradient index (SL), the ratio of valley floor width to valley height (Vf), Basin Shape factor (Bs), and relative index of active tectonics (Iat). Based on results of Iat measures, the tectonic activity of the Anar fault system is higher in the central part (with Iat class from 1 to 2), in comparison with the margins of the study area. This clearly shows that the geomorphic characteristics in the region have been affected by the tectonic activity of the Anar fault system. The morphotectonic analysis carried out to enlighten possibility of reconstruction tectonic activity evidence in the areas with lack of earthquake data.

**Keywords:** neotectonics, morphotectonic analysis, geomorphic indicators, Anar fault system, Yazd block, index of active tectonic

**DOI:** 10.1134/S0016852123040076

## INTRODUCTION

More than half a century of studying the tectonics of Iran shows that the Iranian plateau is a very active part of the Alpine–Himalayan orogenic belt, which is characterized by sophisticated folding and active reverse faulting, recent volcanism, and elevated exposures [2, 3]. Long-term active convergence between the Arabia and Eurasia plates with a velocity rate of 2.1–2.5 cm/yr is ensured to continuous crustal deformation in the forms of thickening, shortening, and active faulting in Iran [3, 18, 19].

As a tectonic sub-continent in the form of a triangle enclosed by large-scale faults, Central Iran has a long history of responding to these tectonic processes. During tectonic activities due to orogenic events, it has played an important role in the formation of current geomorphic features of Iran [20]. The subsequent tectonic phases resulted in forming or reactivating major fractures and basement faults such as Anar, Dehshir, and Chapdoni faults, which have left evidence of geomorphic landscapes in this area.

Our knowledge is poor and some issues remain a challenge about some major structures and their seismicity in the Central Iran such as the Anar fault system due to existing gaps in the historic records of earthquakes could either be due to their location in remote,

arid, sparsely populated areas or a long recurrence period [4].

In this research, it is worth studying tectonics related to geomorphology using morphotectonic tools. The study of these geomorphic landscapes using morphotectonic indicators introduced a deeper insight into the importance and impact of tectonics on the development of the landscape and influencing surface processes in geomorphology. As tectonic geomorphology began to gain significance, there was also a growing interest in neotectonics and active tectonics. In terms of active tectonics, morphometric indices, and geomorphometry have been developed and used many times by authors [1, 8, 11–16, 26, 28, 30], relative tectonic in the Beijing Mountain area in China [6], Northwestern Zagros Mountains in Kurdistan Region of Iraq [35], morphotectonics of Alborz province (Iran) [28], Shekarab Mountains in Eastern Iran [10], Central Kopeh-Dagh in Northeastern Iran [9]). We aim to access the tectonic activity of the fault using morphometric indices in 36 sub-basins along the north termination of the Anar fault system.

The purpose of this work is to implement some morphometric indices in the northern terminal of the Anar fault system within the Yazd block in order to

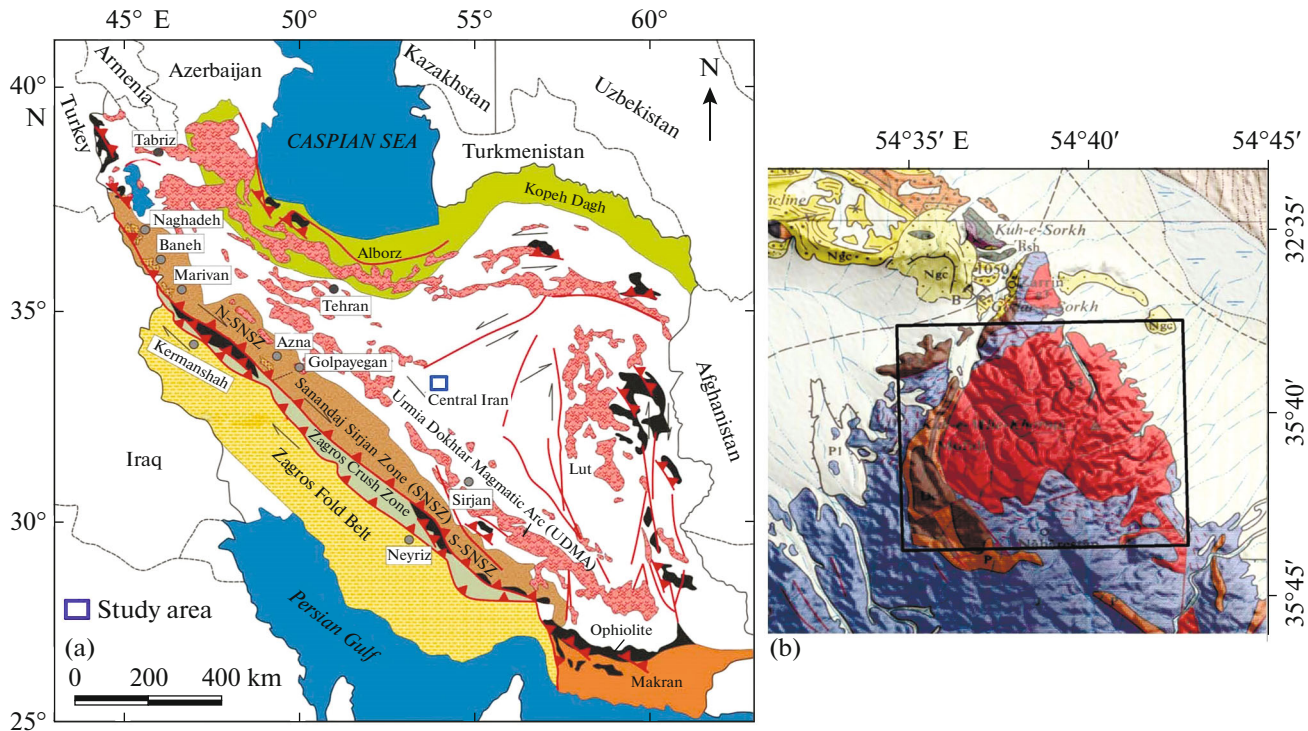


**Fig. 1.** Location of the study area in the Structural map of Iran (after [27, 37], modified). (a) Structural geology map of Iran; (b) Geological map of Ardekan.

investigate relative tectonic activity in the segments of this fault system.

### GEOLOGICAL SETTING

The study area belongs to the Yazd block as a structural unit in the area that forms the central part of Iran called Central–East Iranian Microcontinent (CEIM) [29] (Fig. 1). The Yazd block is located in the southwestern CEIM and is surrounded by the Anar, Dehshir, and Great Kavir (Doruneh) faults at the east, west, and north respectively, and implicates accommodation of Cenozoic convergence by block rotation about vertical axes within the Arabia–Eurasia collision zone [4, 20].

Paleomagnetic studies on the CEIM [23] documented block rotations of Oligocene–Miocene sedimentary units, suggesting that extensive pure shortening along the main faults in Paleogene changed to strike-slip tectonics may have occurred in the Early to Late Miocene [4, 25].

The Anar fault system with a mainly right-lateral strike-slip mechanism and general NNW–SSE trending splays to several minor faults; the northern terminal of the Anar fault cross-cutting Zarin granite in the Kharanagh mountains range at the east of Yazd city and its southern part continues along the foothills to the Anar Salt Plan [24]. This system is a regional-scaled structure subparallel to the Dehshir fault in the

west and the Kuhbanan fault in the east with a length of more than 200 km and geological displacement reported by a minimum of 30 km over the last 20–12 Ma [4, 25, 32].

The current measured slip rate is  $2 \text{ mm} \pm 0.7 \text{ mm/yr}$  whereas a short-term Holocene slip rate of 0.5–0.75 mm/year, with a calculated minimum slip rate of 0.80.1 mm/year [4, 22, 25, 34].

According to Yamani et al. [34] the Anar playa border in the southern part of the Anar fault shows ~1000 and ~40 m of horizontal and vertical offsets, respectively, while the estimated average offset in the north of Anar is ~11.5 m that is new evidence of morphotectonic in the Late Holocene. The deflection of the drainage network along this fault, the cutting of Quaternary sediments in the Anar Desert, the trace of fault slip on the fault surface, the uplift of the Neogene molasse deposits, the Quaternary alluvial terraces and other active geomorphic features in the piedmont area, all of them indicate the activities of the Anar fault during the Quaternary period, while there is no accurate seismic data for this fault [32].

The oldest rock unit is equivalent to the Rizo series with Precambrian age and includes tuff, sandstone, and shale sequences, which are exposed as tectonic windows in Trias to Jurassic units. Sandstone and shale of Shemshak formation is the host rock unit which later post-Jurassic granites emplaced within them. Shearing during the latest tectonic phase (Early

**Table 1.** The values and classes of Bs index in the study area

Sub-basin no.	Value of Bs	Class of Bs	Sub-basin no.	Value of Bs	Class of Bs
b1	2.312	3	b19	2.70353	3
b2	1.916	3	b20	3.2709	2
b3	3.4912	2	b21	1.23339	3
b4	1.2881	3	b22	2.0389	3
b5	3.2463	2	b23	3.0125	2
b6	2.46304	3	b24	3.2981	2
b7	2.787	3	b25	3.1962	2
b8	2.0752	3	b26	1.8816	3
b9	2.6478	3	b27	1.7393	3
b10	1.9061	3	b28	1.5503	3
b11	4.16846	1	b29	2.1177	3
b12	2.6045	3	b30	2.3901	3
b13	2.62597	3	b31	4.1526	2
b14	1.6417	3	b32	2.6776	3
b15	1.466	3	b33	4.3646	2
b16	2.2551	3	b34	1.249	3
b17	2.0084	3	b35	1.2655	3
b18	2.1364	3	b36	8.2692	1

to Late Miocene [4, 25]) also caused mylonitization in the granitic rocks adjacent to the splays of the Anar fault system (Fig. 2).

### MORPHOMETRIC ANALYSIS

In order to investigate the tectonic activities of the Anar fault system, we selected a part of the Kavir (Playa in Persian) Rig-E Zarin basin with an area of 1300 km where the Anar fault is bifurcated. For geomorphic analysis in this work, we prepared required layers such as lithological map, geological structures map, and digital topography models. We performed all processes using Geographic Information System (GIS) software package [36]. Hydrological layers were extracted from projected SRTM with a spatial resolution 30 m into WGS84 UTM of Iran by some preprocessing and processing using the Arc Hydro extension in ArcMap v.10.4.1 environment [36]. Geological and structural maps were digitized based on the detailed maps at 1 : 100000 scale provided by the Geological Survey of Iran [37] and field work geological information. The study area with 36 sub-basins has been evaluated by basin shape factor (Bs), asymmetry factor (Af), stream length-gradient index (SL, and curve and valley floor width-to-height ratio (Vf). According to El Hamdouni [8], average values of each index for 36 sub-basins have been calculated and then, the relative tectonic activity index (Iat) was classified.

### MORPHOTECTONIC INDICES

#### *Basin Shape Index (Bs)*

During landscape development, the shape of the basin is modified through the interaction between tectonic and erosional processes. A relatively young watershed tends to extend to the topographic slope and where tectonic deformation is dominated. With the considerable dominance of erosion over tectonic activities, the elongated shape of the basins tends to evolve circularly.

The Basin shape index (Bs) was developed for the relative tectonic activity and is expressed by the following formula [8]:

$$Bs = B_l/B_w, \quad (1)$$

where  $B_l$  is the distance from the source to the mouth as the target basin length, and  $B_w$  is the width of the basin at its widest part.

Values greater than 4 are concurrent with higher tectonic activity,  $4 < Bs < 3$  with moderate relative activity, and  $Bs < 3$  with low activity. Among the 36 sub-basins, 10 sub-basins have a high value of this parameter, which can indicate high relative active deformation, and are classified into classes 1 and 2 (Table 1, Fig. 3).

#### *Asymmetric Factor (Af)*

Catchment asymmetry analysis helps to identify areas affected by active tectonics such as active folds

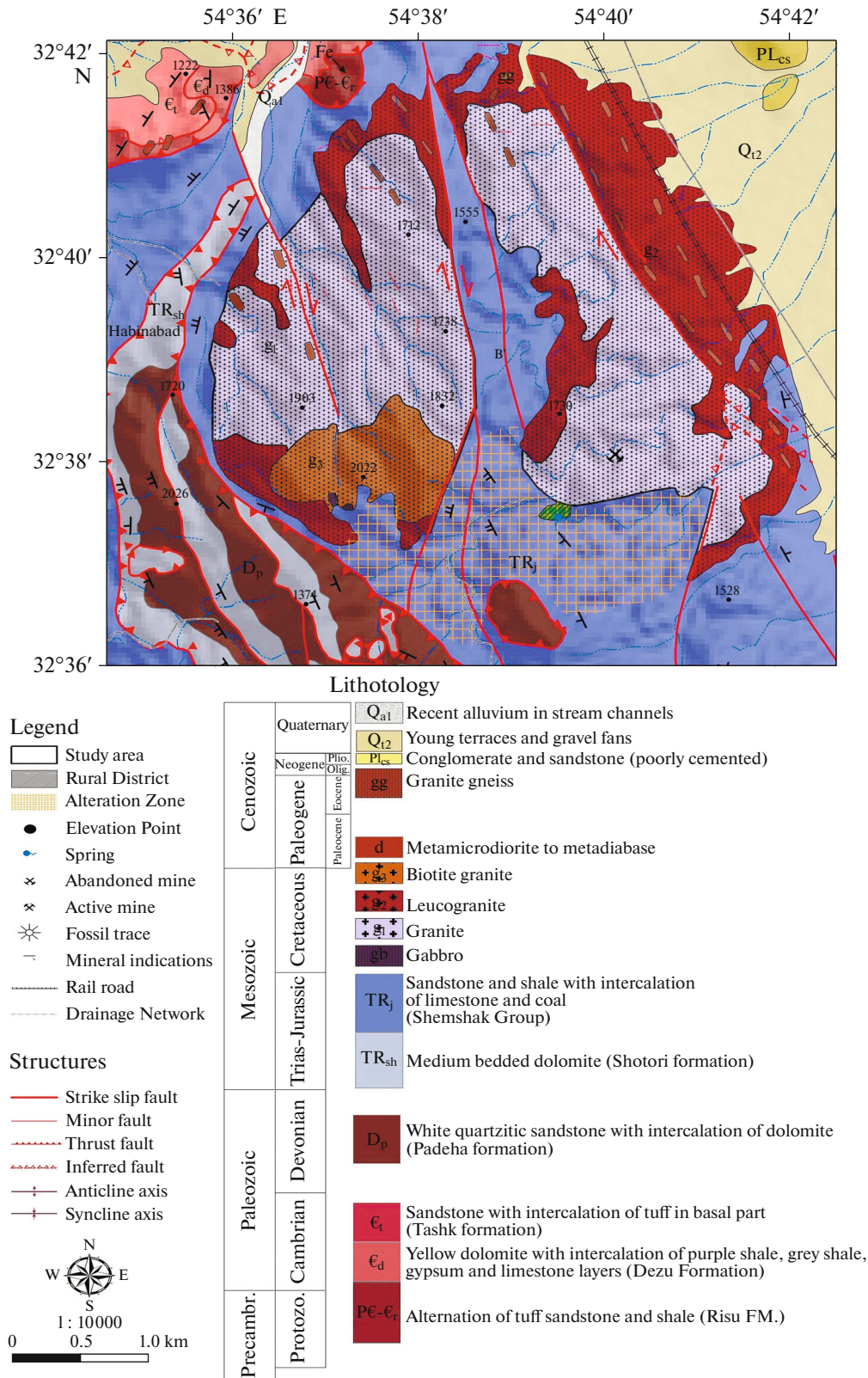
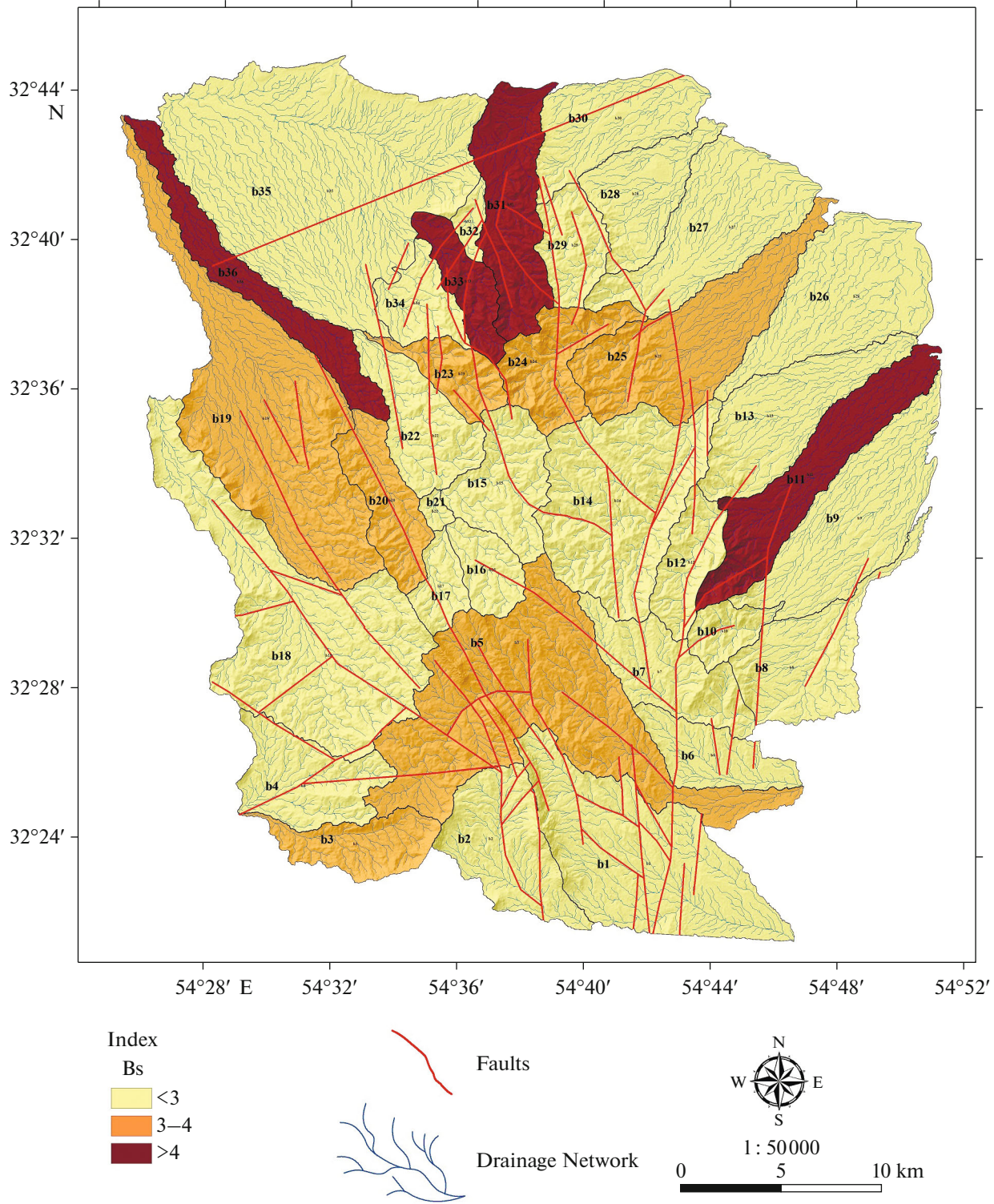


Fig. 2. Geological map of the north terminal of the Anar fault (after [37], modified).



**Fig. 3.** Bs index map of the study area. Based on the BS map, sub-basins 11, 33, 34, and 36 indicate high values of BS index.

and faults. For this purpose, a quantitative tool called the asymmetry factor (Af) was identified by Keller and Pinter [21] and calculated:

$$Af = 100 \times (A_r / A_t), \quad (2)$$

where  $A_r$  is the area of the basin on the right of the main stream (towards downstream) and  $A_t$  is the area of the entire drainage basin. The difference between the neutral value of 50 and the value obtained from the formula above is used as  $Af-50$  to qualitatively express

**Table 2.** The values and classes of Af index in the study area

Sub-basin no.	Value of Af	Class of Af	Sub-basin no.	Value of Af	Class of Af
b1	8	2	b19	13	2
b2	2	3	b20	10	2
b3	32	1	b21	13	2
b4	4	3	b22	19	1
b5	10	2	b23	6	3
b6	10	2	b24	23	1
b7	26	1	b25	3	3
b8	7	3	b26	9	2
b9	16	2	b27	2	3
b10	2	3	b28	13	2
b11	2	3	b29	25	1
b12	2	3	b30	24	1
b13	19	1	b31	8	2
b14	24	1	b32	5	3
b15	12	2	b33	2	3
b16	2	3	b34	17	1
b17	10	2	b35	18	1
b18	7	3	b36	6	3

the results based on relative tectonic activity. High values of Af-50 are related to tectonic activity or lithological structures controls [8].

The lithological effect includes weak surfaces and tendency to slip (bedding or schistosity) in the Af-50 analysis considered in watersheds. Based on Af map of the study area, sub-basins 3, 7, 9, 13, 14, 22, 24, 29, 30, 34, and 35 indicate high values of Af index and have asymmetric shapes (Table 2, Fig. 4).

#### *Stream Length–Gradient Index (SL)*

The estimation of the SL index initiates with the formation of individual stream cross-segments. They were later on separated into portions, which can be outwardly approximated by a straight line. In this parameter, Hack [17] attempted to show the evolution of the landscapes and find out the role of superimposed factors using the stream longitudinal profiles and it is calculated as follows [30]:

$$SL = \Delta h / \Delta l, \quad (3)$$

where  $\Delta h / \Delta l$  is the local slope of the given channel length for evaluation, and  $l$  is the horizontal distance on the channel from the initiation point of the channel to the midpoint of the given segment.

The stream length-gradient index (SL) is widely used in geomorphological studies in order to detect knick-zones where the stream gradient shows anomalous values. The knick-zones are broad deviation along the stream from the typical concave upturned

shape assumed in the longitudinal profile of the stream at a steady state. The value of the SL index depends entirely on the lithology and active deformation, thus the high value of SL ( $\geq 500$ ) as anomalous values usually are related to:

- surface lithology resistance to erosional processes;
- active faulting or folding as subsurface processes;
- slope failures where directly shed the stream channels.

However, the SL value may indicate a decreasing trend ( $< 300$ ) with flowing on low rock resistivity or strike-slip faults [1, 8, 31].

In this work, the range of SL values for the 36 sub-basins is between 90 (sub-basin 26) to 505 (sub-basin 24) determined from digital elevation models (DEM) [38] and geographic information system (GIS) [36] and are indicated in Table 3 and Fig. 5.

Based on the SL map, sub-basins 15 and 24 indicate high tectonic activity.

#### *Ratio of Valley Floor Width to Valley Height (Vf)*

According to Bull and McFadden [5], Vf is described as a geometric index to estimate the shape of a valley to understand the rate of incision versus uplift and is computed by the ratio of the width of the valley floor to its average height through the following expression [5, 8]:

$$Vf = 2V_w / [(E_{ld} - E_{sc}) + (E_{rd} - E_{sc})], \quad (4)$$

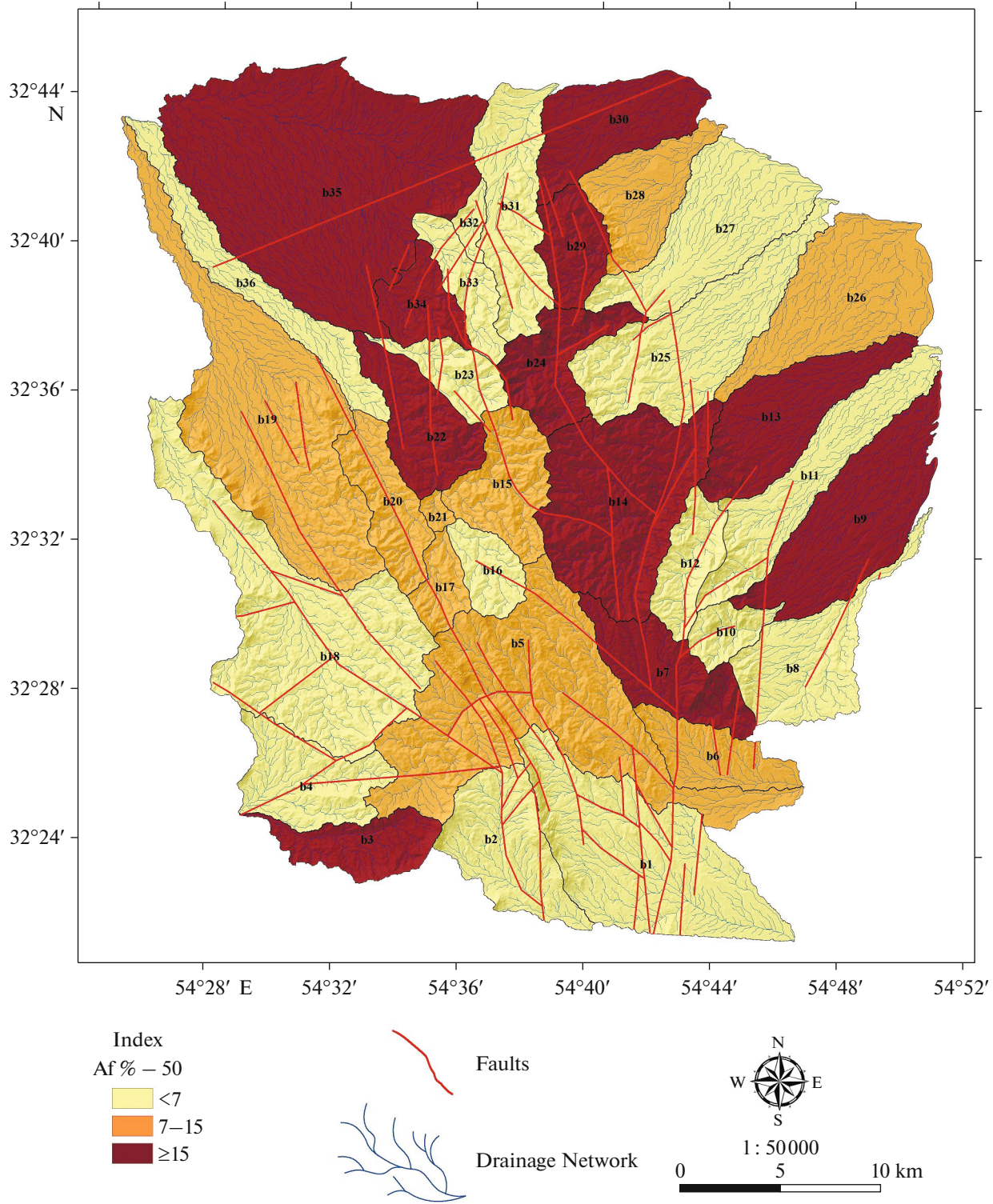


**Fig. 4.** Af index map of the study area. Based on the Af map, sub-basins 3, 7, 9, 13, 14, 22, 24, 29, 30, 34, and 35 indicate high values of Af index.

where  $E_{ld}$  and  $E_{rd}$  are the left and right elevations of the drainage,  $V_w$  is the width of valley floor, and the valley floor elevation is marked with  $E_{sc}$ . This geometric

index by values greater than one represents U-shape valleys, while narrow (V-shape) valleys are detected with Vf values less than one [7].

**Table 3.** The values and classes of SL index in the study area

Sub-basin no.	Value of SL	Class of SL	Sub-basin no.	Value of SL	Class of SL
b1	396.17	2	b19	429	2
b2	310.7	2	b20	347	2
b3	274	3	b21	114	3
b4	232	3	b22	367	2
b5	481	2	b23	396	2
b6	250	3	b24	505	1
b7	317	2	b25	389	2
b8	353	2	b26	90	3
b9	252	3	b27	227	3
b10	375	2	b28	156	3
b11	495	2	b29	356	2
b12	495	2	b30	117	3
b13	286	3	b31	398	2
b14	332	2	b32	145	3
b15	504	1	b33	457	2
b16	326	2	b34	355	2
b17	309	2	b35	226	3
b18	314	2	b36	187	3

**Table 4.** The values and classes of Vf index in the study area

Sub-basin no.	Value of Vf	Class of Vf	Sub-basin no.	Value of Vf	Class of Vf
b1	1.4	3	b19	2.8969	3
b2	0.686	2	b20	0.6993	2
b3	1.196	3	b21	0.8011	2
b4	1.08	3	b22	1.147	3
b5	0.404	1	b23	0.9052	2
b6	4.904	3	b24	0.3432	1
b7	0.491	1	b25	66.28	*
b8	12.204	*	b26	773.037	*
b9	20.155	*	b27	100.62	*
b10	0.19	1	b28	30.903	*
b11	0.92	2	b29	0.4263	1
b12	0.92	2	b30	106.55	*
b13	15.37	*	b31	1.174	3
b14	0.29	1	b32	3.119	3
b15	0.3396	1	b33	3.706	3
b16	0.2283	1	b34	24.027	*
b17	0.6817	2	b35	30.64	*
b18	1.2807	3	b36	25.814	*

For calculating this parameter, we used the projected SRTM to extract areas with a slope of less than 12.5% as a flat valley floor around the mainstream for each sub-basin, then the orthogonal lines to the main

streams were drowned at intervals of 1000 m along the streams and finally the required elevation points ( $E_{ld}$ ,  $E_{rd}$ , and  $E_{sc}$ ) using of the extraction toolset among the spatial analyst toolbox in ArcMap v.10.4.1 [36]. The



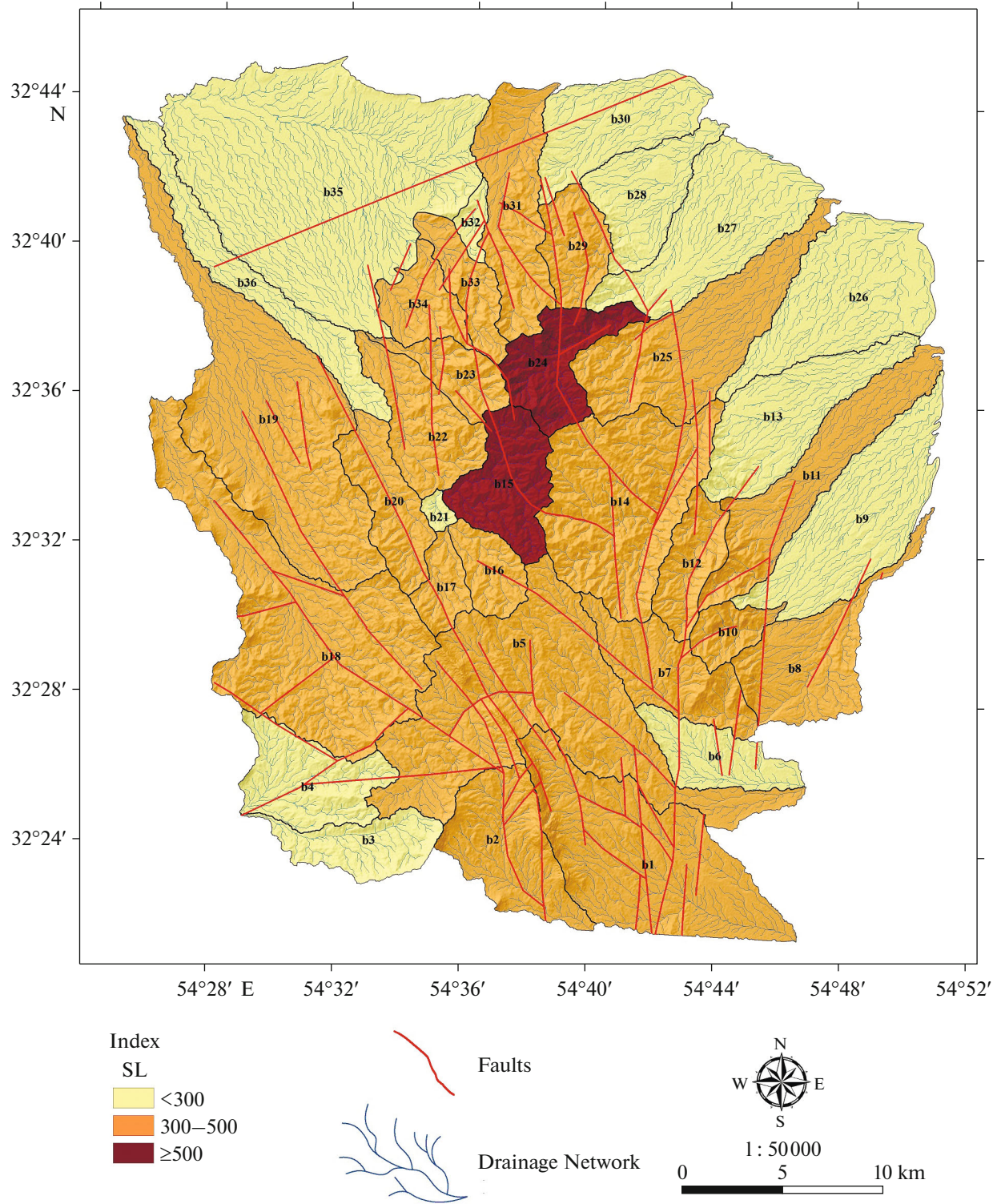


**Fig. 5.** SL index map of the study area. Based on the SL map, sub-basins 15 and 24 indicate high values of SL index.

values of VF based on the relative active tectonics are classified into three classes (Table 4, Fig. 6):

— class 1 (high tectonic activity) with values less than 0.5;

— class 2 (moderately active tectonics) with values between 0.5 and 1;

— class 3 (low active or inactive) with values greater than 1.

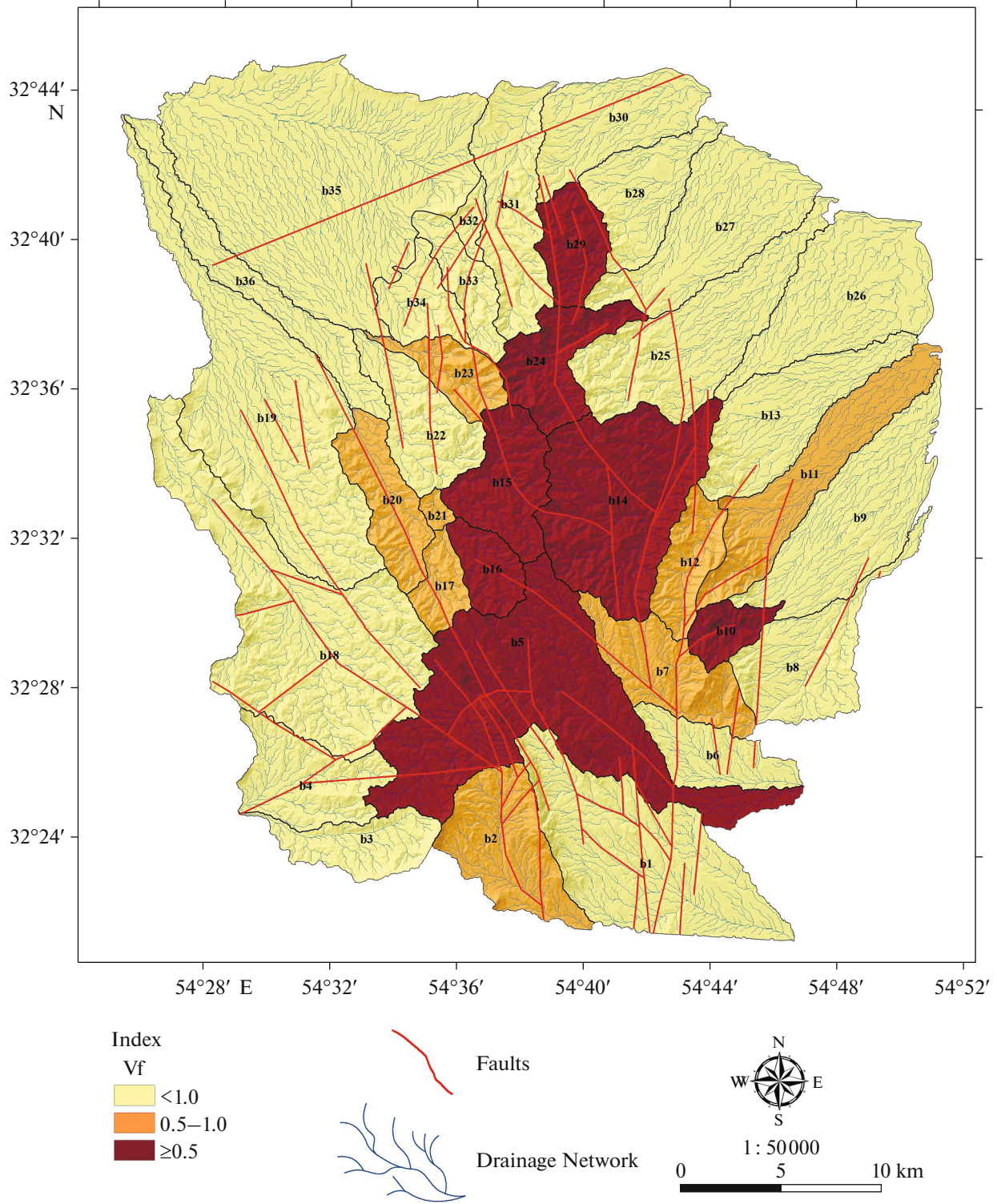


Fig. 6. Vf index map of the study area. Based on the Vf map, sub-basins 5, 10, 14, 15, 16, 24, and 29 indicate high values of Vf index.

*Relative Index of Active Tectonics (Iat)*

This index is evaluated by averaging different classes of morphometric indices for each drainage basin (S/n) and is divided into four classes (Table 5).

Based on the Iat map, Sub-basin 24 shows (in dark red) very high tectonic activity (class 1). Basins 5, 7, 14, 15, and 29 show high tectonic activity (class 2); and the rest of the basins are in classes 3 and 4 (Table 6, Fig. 7).

**Table 5.** Classification of S/n (after [8])

S/N	Class	Description
$\geq 2.5$	4	Low tectonic activity
$2 \leq S/N < 2.5$	3	Moderately tectonic activity
$1.5 \leq S/N < 2$	2	High tectonic activity
$S/N < 1.5$	1	Very high tectonic activity

## DISCUSSION

The Anar fault, with approximately 200 km length, is one of the active faults in the Central Iran; this fault has 0.8 mm/year slip movement rate and mechanism of it has not been well understood and remains a challenge [24]. Investigation of the geomorphic evidence along the Anar fault shows that the Anar fault is active; because there are many evidence of its activity in the late Holocene time [34].

Although, based on earthquake maps the Dehshir and Anar faults have not had considerable earthquakes ( $M_b \geq 4.5$ ) but there is much notable evidence of neotectonic movements the in the Quaternary landforms around it [22, 25, 34].

Furthermore, lack of historical seismic records does not indicate absence of seismic activity along these faults. The Central Iran landforms are strongly influenced by the movements of the recent fault (particularly strike-slip faults).

Despite the lack of seismicity in the vicinity of the Anar fault, there is clear morphological evidence that

the Anar fault is active [22, 25]. Existing of springs along the Dehshir and Anar faults demonstrates that these faults were active since they stretched as a linear form of shape [34].

The Anar fault displaced the border of the Anar playa ~1000 m and caused a sharp scarp analogous a wall-like feature with ~40 m high. In the northern part of the Anar fault 11.5 m offset is estimated and it shows new evidence of morphotectonic movements in the Late Holocene [34]; the field view of the Anar fault is shown in Fig. 8. In order to estimate the tectonic activity of the Anar fault we used morphotectonic analysis.

Firstly, we determined 36 sub-basins in the study area, and morphometric indices were calculated for these sub-basins which are located along the northern terminal of the Anar fault system within the Yazd block. Measured indices including Af, Vf, Bs, SL, and S/n shows that the north terminal of the Anar fault is currently active. Based on the calculation of relative index of active tectonics (Iat) (Fig. 7):

- the sub-basin 24 have a very high tectonic activity (class 1);
- the sub-basins 5, 7, 14, 15, and 29 show high tectonic activity (class 2);
- the rest of the basins are located in classes 3 and 4.

Moreover, the sub-basins which show the high rates of tectonic activity are related to the places where densities of the faults are high (Fig. 8).

Active faulting in the study area is prime responsible for a variety of landform features, including fault

**Table 6.** The values and classes of S/n index in the study area

Sub-basin no.	Value of S/n	Class	Sub-basin no.	Value of S/n	Class
b1	2.2	3	b19	2.4	3
b2	2.4	3	b20	2.2	3
b3	2.2	3	b21	2.2	3
b4	2.8	4	b22	2.2	3
b5	1.8	2	b23	2.2	3
b6	2.8	4	b24	1.4	1
b7	1.6	2	b25	2.5	4
b8	2.5	4	b26	2.5	4
b9	2.5	4	b27	2.5	4
b10	2	3	b28	2.75	4
b11	2	3	b29	1.6	2
b12	2.4	3	b30	2.5	4
b13	2	3	b31	2.4	3
b14	1.6	2	b32	2.6	4
b15	1.8	2	b33	2.6	4
b16	2.2	3	b34	2.25	3
b17	2.4	3	b35	2.5	4
b18	2.8	4	b36	2.5	4

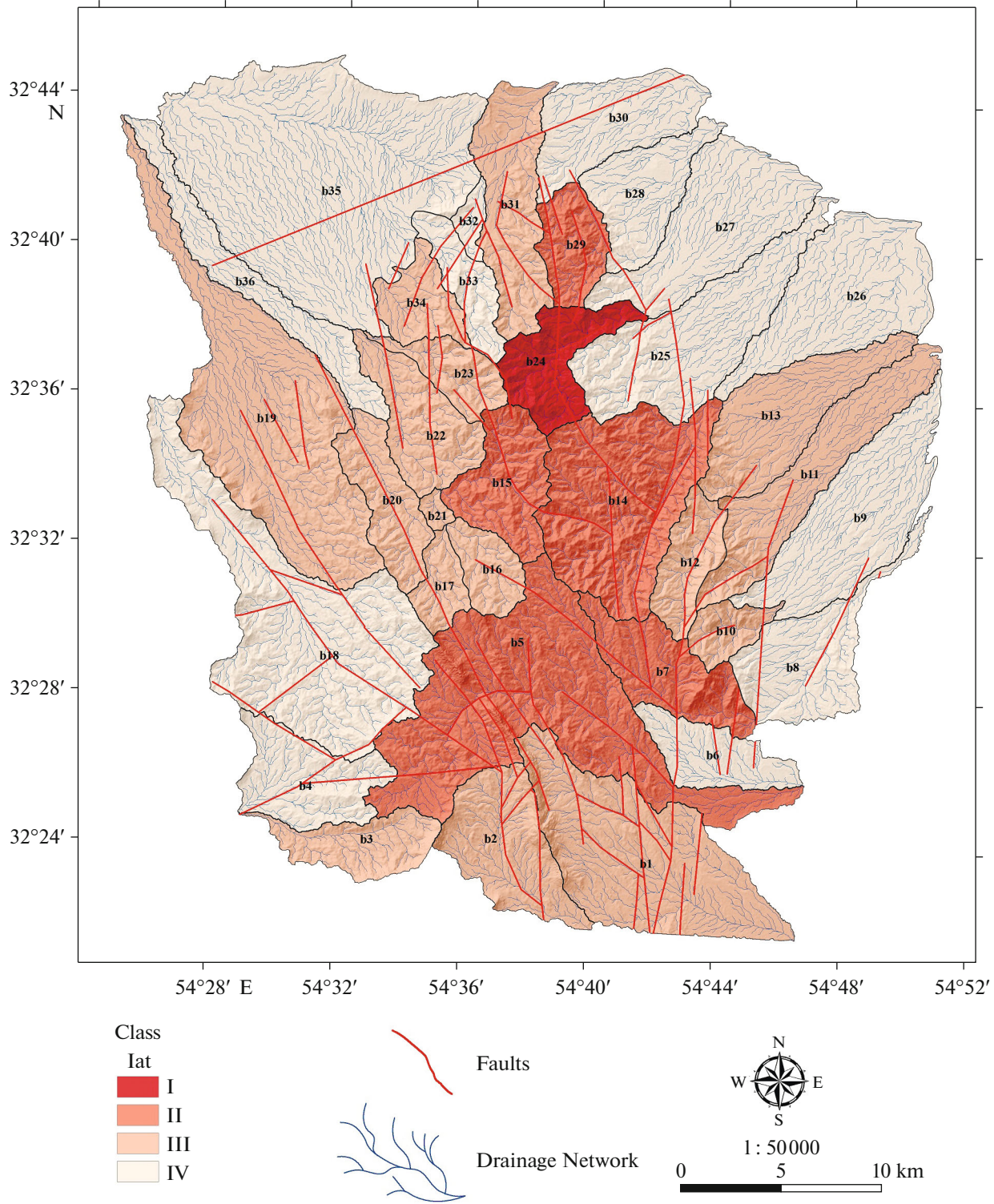


**Fig. 7.** Iat map of the studied drainage basins. Sub-basin 24 shows (dark red) very high tectonic activity (class 1); sub-basins 5, 7, 14, 15, and 29 show high tectonic activity (class 2); and the rest of the basins along the faults are in classes 3 and 4.

scarps and traces, warped and tilted slopes, fault springs, vegetation lineation, and offset features such as stream channels which they are indicators of the active tectonics in the region [21]. Deformation of the

Playas, travertine deposits, drainage patterns, and alluvial fans occur in the study area; they are consequences of the landscape dynamical activity in the study area [34]. Field observations and investigation of

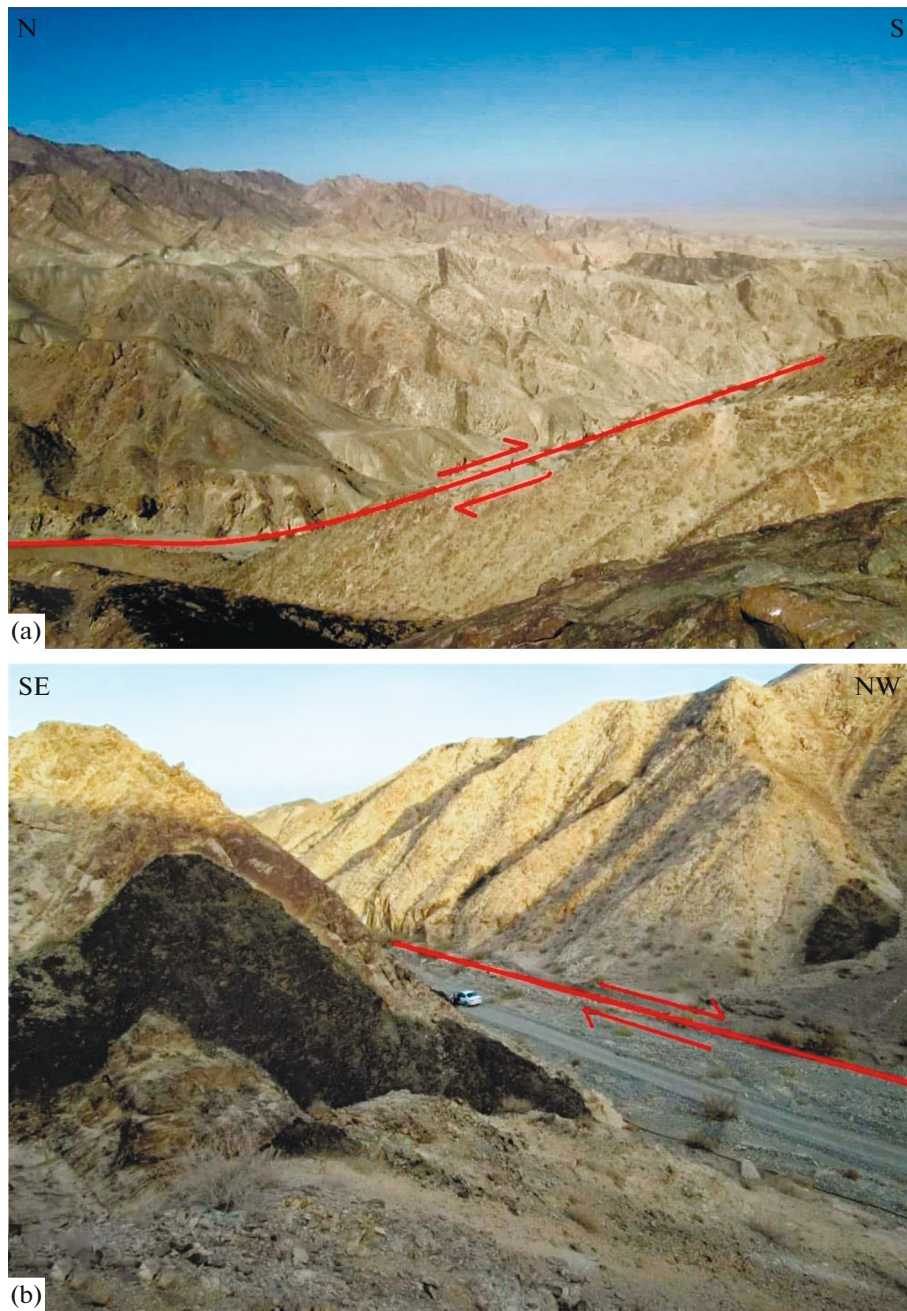


Fig. 8. The right-lateral strike-slip Anar fault. Field view: (a) N–S; (b) ES–NW.

morphotectonic indicators in the present study show that the Central Iran is not a completely stable block, and its dominant deformation has the ability to create a significant seismic hazard. Therefore, the production of rare and large earthquakes is one of the characteristics of the strike-slip faults in Central Iran, such as the Anar fault system.

## CONCLUSIONS

(1) Investigation of the morphometric indices along the North Terminal of the Anar fault in the Cen-

tral Iran plate shows that this area is considered as a tectonically active area, although no significant seismic activity has been reported yet.

(2) Based on active tectonics indices (Iat), in the central part of the study area, where the density of faults is higher, the tectonic activity is also high (Iat class = 1 or 2). Moreover, in the margins of the study area which the density of faults is less as well as the tectonic activity is less.

(3) Morphotectonic analysis performed showed clearly that the geomorphic drainages in the region

had been affected by the activity of the Anar fault coupled with current minor faults.

#### ACKNOWLEDGMENTS

The authors are thankful to Mrs. Leila Hashemi Dehsarvi (Shiraz University, Shiraz, Iran) for friendly help and very practical recommendations in using morphotectonic methods. Special thanks to Dr. Raana Razavi Pash (Shiraz University, Shiraz, Iran) for his helpful advices and comment. We also thank to Dr. Maryam Ezati (University of Birjand, Birjand, Iran) for grammar review of the manuscript. The authors are also grateful to reviewer Prof. V.G. Trifonov (GIN EAS, Moscow, Russia) and an anonymous reviewer for helpful comments and editor M.N. Shoupletsova (GIN RAS, Moscow, Russia) for thorough editing.

#### FUNDING

This research was supported by the University of Birjand Research Council ((BURC), Iran) grant which is gratefully acknowledgment.

#### CONFLICT OF INTEREST

The authors declare that they have no conflict of interest.

#### REFERENCES

1. R. Alipoor, M. Poorkermani, M. Zare, R. El-Hamdouni, "Active tectonic assessment around Rudbar Lorestan dam site, High Zagros Belt (SW of Iran)," *Geomorphology* **128**, 1–14 (2011).
2. M. Berberian and S. Arshadi, "On the evidence of the youngest activity of the North Tabriz fault and the seismicity of Tabriz city," *Geol. Surv. Iran Rep.* **39**, 397–418 (1976).
3. M. Berberian and G. C. P. King, "Towards a paleogeography and tectonic evolution of Iran," *Can. J. Earth Sci.* **18**, 210–265 (1981).
4. M. Berberian, "Active tectonics and geologic setting of the Iranian Plateau," *Develop. Earth Surf. Proc.* **17**, 151–171 (2014).
5. W. B. Bull and L. M. McFadden, "Tectonic geomorphology north and south of the Garlock fault, California," *J. Geomorphol.* **1**, 15–32 (1977).
6. W. Cheng, N. Wang, M. Zhao, and Sh. Zhao, "Relative tectonics and debris flow hazards in the Beijing Mountain area from DEM-derived geomorphic indices and drainage analysis," *Geomorphology* **257**, 134–142 (2016).
7. H. Daxberger, R. Dalumpines, D. M. Scott, and U. Riller, "The ValleyMorph Tool: An automated extraction tool for transverse topographic symmetry (T-) factor and valley width to valley height (Vf) ratio," *Comp. Geosci.* **70**, 154–163 (2014).
8. R. El-Hamdouni, C. Irigaray, T. Fernández, J. Chacón, and E. A. Keller, "Assessment of relative active tectonics, southwest border of the Sierra Nevada (Southern Spain)," *Geomorphology* **96**, 150–173 (2008).
9. M. Ezzati and E. Gholami, "Neotectonics of the Central Kopeh Dagh drainage basins, NE Iran," *Arab. J. Geosci.* **15**, 1–18 (2022).
10. M. Ezzati, E. Gholami, and S. M. Mousavi, "Tectonic activity level evaluation using geomorphic indices in the Shekarab Mountains, Eastern Iran," *Arab. J. Geosci.* **14**, 1–385 (2021).
11. A. Faghih, A. Esmailzadeh Soudejani, A. Nourbakhsh, and S. Rokni, "Tectonic geomorphology of High Zagros Ranges, SW Iran: An initiative towards seismic hazard assessment," *Environ. Earth Sci.* **74**, 3007–3017 (2015).
12. A. Faghih, I. Nezamzadeh, and T. Kusky, "Geomorphometric evidence of an active pop-up structure along the Sabzpushan Fault Zone, Zagros Mountains, SW Iran," *J. Earth Sci.* **27**, 945–954 (2016).
13. A. Faghih and A. Nourbakhsh, "Implication of surface fractal analysis to evaluate the relative sensitivity of topography to active tectonics, Zagros Mountains, Iran," *J. Mountain Sci.* **12**, 177–185 (2014a).
14. A. Faghih and A. Nourbakhsh, "Appraisal of relative tectonic activity along the Kazerun Fault Zone, Zagros Mountains, Iran: Insight from spatial analysis of geomorphic indices," *Geol. J.* **50**, 783–798 (2014b).
15. A. Faghih, A. Nourbakhsh, and T. Kusky, "GIS-based analysis of relative tectonic activity along the Kazerun Fault Zone, Zagros Mountains, Iran: Insights from data mining of geomorphic data," *J. Earth Sci.* **26**, 712–723 (2015).
16. A. Faghih, B. Samani, T. M. Kusky, S. Khabazi, and R. Roshanak, "Geomorphologic assessment of relative tectonic activity in the Maharlou Lake Basin, Zagros Mountains of Iran," *Geol. J.* **47**, 30–40 (2012).
17. J. T. Hack, "Stream-profile analysis and stream-gradient index," *USGS Res. J.* **1**, 421–429 (1973).
18. K. Hessami and F. Jamali, "Explanatory notes to the map of major active faults of Iran," *J. Seism. Earthquake Eng.* **8**, 1–11 (2006).
19. J. Jackson and D. McKenzie, "Rotational mechanisms of active deformation in Greece and Iran," *Spec. Publ.—Geol. Soc. London* **17**, 743–754 (1984).
20. F. Kargaranfaghghi, F. Neubauer, and J. Genser, "Cenozoic kinematic evolution of southwestern Central Iran: Strain partitioning and accommodation of Arabia–Eurasia convergence," *Tectonophysics* **502**, 221–243 (2011).
21. E. A. Keller and N. Pinter, *Active Tectonics* (Upper Saddle River, NJ: Prentice Hall, 1996, **Vol. 338**).
22. K. Le Dortz, B. Meyer, M. Sébrier, H. Nazari, R. Braucher, M. Fattahi, L. Benedetti, M. Foroutan, L. Siame, D. Bourlès, and M. Talebian, "Holocene right-slip rate determined by cosmogenic and OSL dating on the Anar fault, Central Iran," *Geophys. J. Int.* **179**, 700–710 (2009).
23. M. Mattei, F. Cifelli, G. Muttoni, A. Zanchi, F. Berra, F. Mossavvari, and S. A. Eshraghi, "Neogene block rotation in central Iran: Evidence from paleomagnetic data," *GSA Bull.* **124**, 943–956 (2012).
24. A. Mehrabi, S. Pirasteh, A. Rashidi, M. Pourkhosravi, R. Derakhshani, G. Liu, W. Mao, and W. Xiang, "Incorporating persistent scatterer interferometry and radon anomaly to understand the Anar Fault mecha-

- nism and observing new evidence of intensified activity,” *Remote Sens.* **13**, 2072–2093 (2021). <https://doi.org/10.3390/rs13112072>
25. B. Meyer and K. Le Dortz, “Strike-slip kinematics in Central and Eastern Iran: Estimating fault slip-rates averaged over the Holocene,” *Tectonics* **26**, 5–25 (2007).
  26. A. A. Misra and S. Mukherjee, “Introduction to atlas of structural geological and geomorphological interpretation of remote sensing images,” in *Atlas of Structural Geological and Geomorphological Interpretation of Remote Sensing Images*, Ed. by A. A. Misra and S. Mukherjee (John Wiley, The Atrium, Southern Gate, Chichester, West Sussex, PO19 8SQ, UK, 2023), pp. 1–5.
  27. J. Stoecklin, “Structural history and tectonics of Iran: A review,” *AAPG Bull.* **52** (7), 1229–1258 (1968).
  28. V. Taesiri, M. Pourkermani, A. Sorbi, M. Almasian, and M. Arian, “Morphotectonics of Alborz province (Iran): A case study using GIS method,” *Geotectonics* **54**, 691–704 (2020).
  29. M. Takin, “Iranian geology and continental drift in the Middle East,” *Nature* **235**, 147–150 (1972).
  30. F. Troiani and M. Della Seta, “Geomorphological response of fluvial and coastal terraces to Quaternary tectonics and climate as revealed by geostatistical topographic analysis,” *Earth Surf. Proc. Landforms* **36**, 1193–1208 (2011).
  31. F. Troiani, J. P. Galve, D. Piacentini, M. Della Seta, and J. Guerrero, “Spatial analysis of stream length-gradient (SL) index for detecting hillslope processes: A case of the Gállego River headwaters (Central Pyrenees, Spain),” *Geomorphology* **214**, 183–197 (2014).
  32. R. Walker and J. Jackson, “Active tectonics and late Cenozoic strain distribution in Central and Eastern Iran,” *Tectonics* **23**, 1529–1553 (2004).
  33. A. Walpersdorf, I. Manighetti, Z. Mousavi, F. Tavakoli, M. Vergnolle, A. Jadidi, D. Hatzfeld, A. Aghamohammadi, A. Bigot, Y. Djamour, and H. Nankali, “Present-day kinematics and fault slip rates in eastern Iran, derived from 11 years of GPS data,” *J. Geophys. Res.: Solid Earth*, **119**, 1359–1383 (2014).
  34. M. Yamani, A. Goorabi, and A. Kakroodia, “Evidence of neotectonics along Dehshir and Anar faults in Central Iran by using remote sensing data,” *Wulfenia*, **20**, 1–29 (2013).
  35. M. Zebari, Ph. Balling, Ch. Grützner, P. Navabpour, J. Witte, and K. Ustaszewski, “Structural style of the NW Zagros Mountains and the role of basement thrusting for its mountain front flexure, Kurdistan Region of Iraq,” *J. Struct. Geol.* **141**, 104–206 (2020).
  36. Environmental Systems Research Institute (ESRI), Geographic Information System (GIS) Software Package, (ArcMap 10.4.1), <http://www.esri.com> (Accessed April 18, 2015).
  37. Geological map of Ardekan at 1 : 100000 scale. Geological Survey of Iran, <https://gsi.ir/en> (Accessed June 25, 2005).
  38. Digital Elevation Models (DEM), <https://earthexplorer.usgs.gov/> (Accessed December 13, 2022).